*remote sensing*

MDPI

*Article*

# Integration of Optical and Microwave Satellite Data for Monitoring Vegetation Status in Sorghum Fields

**Simone Pilia, Giacomo Fontanelli, Leonardo Santurri, Enrico Palchetti, Giuliano Ramat, Fabrizio Baroni *, Emanuele Santi, Alessandro Lapini, Simone Pettinato and Simonetta Paloscia**

Institute of Applied Physics 'Nello Carrara'—National Research Council (IFAC-CNR), 50019 Florence, Italy; s.pilia@ifac.cnr.it (S.P.); g.fontanelli@ifac.cnr.it (G.F.); l.santurri@ifac.cnr.it (L.S.); e.palchetti@ifac.cnr.it (E.P.); g.ramat@ifac.cnr.it (G.R.); e.santi@ifac.cnr.it (E.S.); a.lapini@ifac.cnr.it (A.L.); s.pettinato@ifac.cnr.it (S.P.); s.paloscia@ifac.cnr.it (S.P.)

* Correspondence: f.baroni@ifac.cnr.it

**Abstract:** Despite the abundance of available studies on optical and microwave methods devoted to investigating agricultural crop conditions, there is a lack of research that explores the integration between microwave and optical data and the link between photosynthetic activity, measured by PRI (photochemical reflectance index), and vegetation water content, detected by radar sensors. In particular, there is a lack of vision that links these measures to better understand how plants react and adapt to possible water stress conditions. Most of the existing research tends to treat optical and microwave information separately, without investigating how the integration of these techniques can provide a more complete and accurate understanding of the research topic, corroborated by ground data. In this paper, an integrated approach using microwave and optical satellite data, respectively acquired by Sentinel-1 (S-1) and Sentinel-2 (S-2), was presented for monitoring vegetation status. Experimental data and electromagnetic models have been combined to relate backscattering from S-1 and optical indices from S-2 to plant conditions, which were evaluated by measuring PRI, plant water content (PWC), and soil water content. Field data were collected in two sorghum fields close to Florence in Tuscany (Central Italy) during the summers of 2022 and 2023. The results show significant correlations between microwave and optical data with respect to field measurements, highlighting the potential of remote sensing techniques for agricultural monitoring and management, also in response to climate change. Determination coefficients of $R^2 = 0.51$ between PRI and PWC, where PWC is retrieved by S-1, and $R^2 = 0.73$ between PSRI (plant senescence reflectance index) and PRI were obtained.

**Keywords:** Sentinel-1; backscattering; Sentinel-2; optical indices; PRI; sorghum; plant water content; water cloud model

check for updates

Academic Editor: Javier J Cancela

Received: 13 March 2025
Revised: 15 April 2025
Accepted: 27 April 2025
Published: 30 April 2025

**Citation:** Pilia, S.; Fontanelli, G.; Santurri, L.; Palchetti, E.; Ramat, G.; Baroni, F.; Santi, E.; Lapini, A.; Pettinato, S.; Paloscia, S. Integration of Optical and Microwave Satellite Data for Monitoring Vegetation Status in Sorghum Fields. *Remote Sens.* **2025**, *17*, 1591. https://doi.org/10.3390/rs17091591

**Copyright:** © 2025 by the authors. Licensee MDPI, Basel, Switzerland. This article is an open access article distributed under the terms and conditions of the Creative Commons Attribution (CC BY) license (https://creativecommons.org/licenses/by/4.0/).

## 1. Introduction

Monitoring crop conditions is essential for optimizing agricultural practices and reducing water waste. The increasing impacts of climate change, with more and more frequent extreme weather events and persistent droughts [1,2], have a strong effect on crop productivity [3], health, and yields [4]. Recently, these risks have been expanding in several regions within the Mediterranean basin [5]. Therefore, effective management of soil and water resources can be considered as a key factor in achieving sustainable food production [6]. In this context, monitoring vegetation from space can greatly enhance our understanding of Earth's surface processes such as hydrological cycle and crop productivity. With the rapid

advancements in remote sensing technology, the estimation of several natural parameters with high spatiotemporal resolution is becoming more and more feasible. Remote sensing techniques support observations of the most important surface characteristics according to different sensors: the optical ones, such as visible-near-infrared [7], hyperspectral [8], and thermal infrared sensing [9], have limited penetration capabilities, making it impossible to obtain soil information in the presence of dense vegetation layers and of the entire vegetation structure in the case of well-developed plants. Nevertheless, the signal in these wavelengths (λ) is very sensitive to vegetation pigments and photosynthetic activity [10]. Furthermore, the use of these sensors is hampered by weather conditions like the presence of clouds [11], rainfall, and solar illumination. Microwave sensors, such as synthetic aperture radar (SAR), have instead a deeper penetration and better capability to observe objects in the absence of solar light and cloud cover. In this wavelength range, the dielectric properties of vegetation are affected both by water content and the geometric characteristics of plants, including the size of leaves, branches, and stems [12]. These elements influence scattering and absorption mechanisms, which vary according to frequency, incidence angle of observation, and polarization [13,14]. Moreover, the electromagnetic response of soil under vegetation greatly influences the backscattering ($\sigma^0$), due its high sensitivity to soil moisture content (SMC) and surface roughness [15]. The dielectric properties govern the interactions of backscatter with the medium through various phenomena such as absorption, scattering, and penetration. The penetration of microwave signal increases at lower frequency, and thus is higher in L- and P-band [16,17].

The launch of the S-1 and S-2 satellites by the European Space Agency (ESA) has significantly increased the possibility of monitoring crop conditions and soil moisture from space [18,19]. S-1, equipped with a C-band SAR, offers all-weather, day-and-night imaging capabilities that are crucial for consistent monitoring of agricultural fields. S-2 provides high-resolution optical imagery by using 13 spectral bands, allowing for detailed assessment of vegetation health and vigor by most widely used vegetation indexes [20].

In this paper, a very important index, i.e., the photochemical reflectance index (PRI), has been taken into consideration because it is widely considered as an indicator of photosynthetic efficiency and productivity and is related to the water-stress index [21]. PRI is obtained from the normalization between the difference of reflectivity at 531 nm and a reference wavelength, typically at 550 or 570 nm, and it is used to assess radiation use efficiency (RUE) at leaf, canopy, and ecosystem levels [22–25]. The consistency of the RUE–PRI relationship suggests a functional convergence in the components affecting carbon uptake efficiencies [26]. Then, complementing NDVI-like indices with PRI can improve the precise monitoring and management of agricultural ecosystems [27]. PRI would be measured in situ by using portable sensors; however, due to the bands needed for its computation, PRI can be derived from MODIS but not from S-2.

Due to the peculiar characteristics of optical and microwave satellite data, the integration of these two types of measurements enables a comprehensive approach for assessing crop health, water status, and soil conditions, by combining different sensitivities, thus obtaining more in-depth information on the canopy [28]. The literature actually shows a lack of research that explores an integration between photosynthetic activity, measured by PRI, and vegetation water content, detected by radar sensors. In particular, there is a lack of a vision that links these measures to better understand how plants react and can adapt to possible water-stress conditions. In light of this analysis, some research gaps emerge. First, there is a lack of a study relating PRI to microwave measurements. Secondly, the temporal variations of these microwave features and their significance for monitoring the changes in vegetation status have not been sufficiently explored. Finally, there is a need for validation to compare these parameters with consolidated indices in the literature to

confirm the reliability and practical utility of the combined method. From these issues, the following questions can be derived. First, what is the specific relationship between photosynthetic activity, measured by PRI, and the water content of vegetation detected by microwave sensors? Second, how do these relationships vary and what implications do they have for understanding plant dynamics?

The experimental results have been confirmed and evaluated by using well-assessed electromagnetic models such as the Water Cloud Model (WCM), which was used for estimating the vegetation water content. Although the WCM was not conceived recently, it is still used at present in remote sensing studies to estimate the water content in the canopy, the aboveground biomass, and the soil moisture [29–33], since it offers a good tradeoff between accuracy and computational cost. In this study, the WCM has been reappraised as proposed in [15], by coupling it with the Integral Equation Model (IEM) [34], the Oh [35], and the Dobson model [36].

In this paper, the vegetation status and health in two sorghum fields close to Florence, Italy, has been evaluated by exploiting on-site measurements of PRI and further integration with the PWC obtained from S-1 data. The analysis and data collection were performed during the summers of 2022 [37] and 2023 [38]. Additionally, we used a series of well-known S-2-derived indices that are sensitive to plant health conditions to confirm their sensitivity to vegetation water status.

The novelty of this research work consists in the simultaneous use of SAR and multispectral data for estimating PWC and PRI. In particular, SAR data have been used as inputs of electromagnetic models such as the WCM and the IEM for retrieving PWC, which in turn was correlated with PRI. Some indices derived from S-2 have also been related to PRI. Another important aspect was the use of morning and afternoon S-1 passes for exploiting the SAR sensitivity to the diurnal variations of PWC and PRI.

The results of this study are expected to contribute to improving agricultural management practices and enhancing the understanding of remote-sensing applications in monitoring crop water status and health.

## 2. Materials and Methods

### *2.1. Test Area*

During the summers of 2022 and 2023, measurement campaigns were carried out in two sorghum fields (Figures 1 and 2). Both fields were flat, rainfed, and located close to Florence, Italy, with the following average coordinates: latitude 43.829625°, longitude 11.151517°; and latitude 43.827674°, longitude 11.149736° [39]. Measurements were performed from 2nd of July to 1st of September in 2022 and from 2nd of July to 2nd of October in 2023. The fields used in the study are owned by the same farmer, who decided to leave a plot uncultivated and sowed the adjacent field. In Figure 2, the field indicated by 2022 was cultivated in 2022, leaving the field indicated by 2023 fallow, and vice versa for 2023. The fields are adjacent to each other, and the effect in observation geometry of satellite acquisitions is negligible. Soil type and topography are identical for both.



(**a**) (**b**)

**Figure 1.** (**a**) Sorghum ripening in 2022. (**b**) Sorghum in the well-developed phase in the same year.

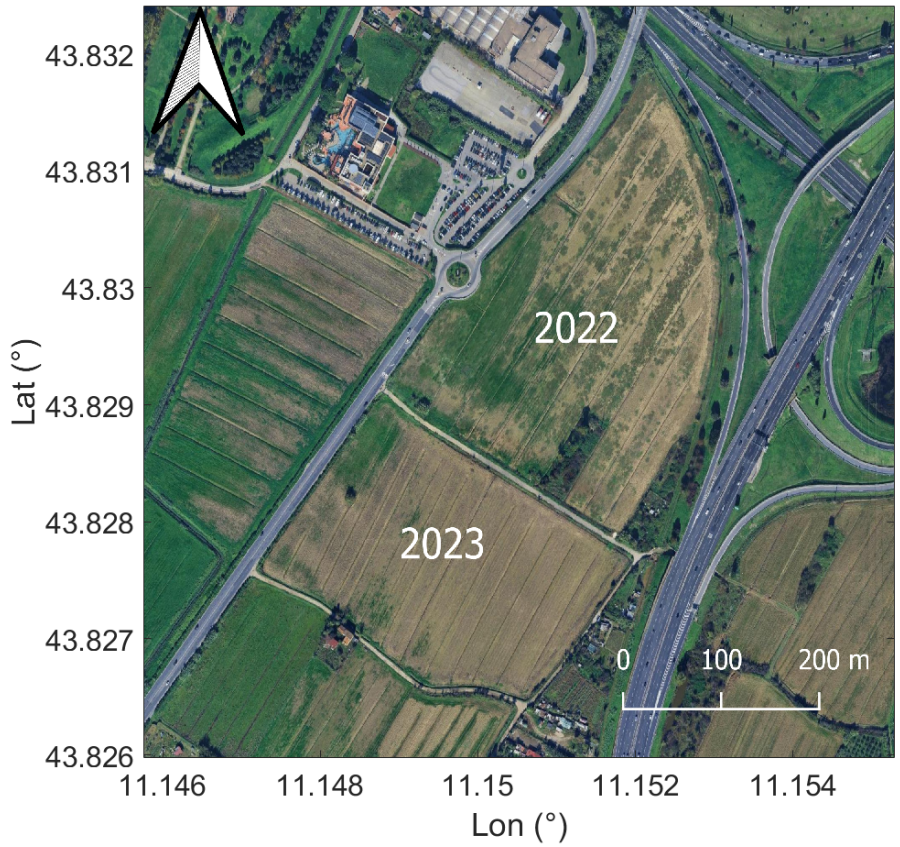



**Figure 2.** Sorghum fields used for the campaigns of 2022 and 2023.

### *2.2. Satellite Data*

S-1 is a constellation of two polar-orbiting satellites, Sentinel-1A (S-1A) and Sentinel-1B (S-1B), sharing the same orbital plane and carrying a SAR in C-band (5.4 GHz). Unfortunately, S-1B experienced an anomaly, causing a halt in the delivery of radar data since the end of 2021, which reduced the revisiting frequency of most of the Earth's surface to 12 days from the original 6 days [40]. The orbits can be of ascending or descending type. Ascending orbits acquire images in the afternoon, while descending orbits do so in the morning. The characteristics of satellite data are reported in Table 1.

**Table 1.** S-1 orbit information.

| S-1 Orbit | Angle of Incidence [deg] | Overpass Time [UTC] |
|---|---|---|
| 117-Ascending | 34.20 | 17:06 |
| 15-Ascending | 43.82 | 17:14 |
| 95-Descending | 43.18 | 05:19 |
| 168-Descending | 33.20 | 05:27 |

S-2 has a temporal resolution of 5 days, overpassing the area at 10:13 UTC (12:13 UTC). S-2 has two identical satellites which operate simultaneously with a phase difference of 180° in a sun-synchronous orbit. The platform provides a total of 13 spectral bands with a spatial resolution ranging between 10 and 60 m. To understand the health status of the sorghum crops in the considered periods, the evolution of the following four S-2 derived indices was analyzed: NDRE (normalized difference red edge index), RGR (red–green ratio), PSRI (plant senescence reflectance index) and SIPI (structure insensitive pigment index) (Table 2). These indices have been selected among many available indices as the most closely related to PRI, showing high determination coefficients ($R^2 > 0.5$–$0.6$), as can be observed in the diagrams and tables of Section 3. Furthermore, as the estimator of the true value the median of all the pixels inside the field was used, as for S-1 data.

**Table 2.** S-1 Indices derived from S-2 bands. $B_2$ = blue (492 nm), $B_3$ = green (559 nm), $B_4$ = red (664 nm), $B_5$ = red edge 1 (704 nm) and $B_8$ = NIR (833 nm).

| Index | Formula | Reference |
|---|---|---|
| NDRE | $\frac{B_8-B_5}{B_8+B_5}$ | [41] |
| RGR | $\frac{B_4}{B_3}$ | [42] |
| PSRI | $\frac{B_4-B_3}{B_8}$ | [43] |
| SIPI | $\frac{B_8-B_2}{B_8+B_4}$ | [44] |

Both S-1 and S-2 data were gathered from Google Earth Engine (GEE). GEE is a cloud computing platform designed for processing satellite imagery and other Earth observation data, with the capability to handle large datasets by distributing computations across multiple servers worldwide [45]. The flowchart of the GEE processing of the S-1 images is represented in Figure 3.




**Figure 3.** Flowchart of the Google Earth Engine processing of the S-1 images.

Users can interact with the platform via an interactive development environment (IDE), using Python and JavaScript libraries [46]. Only L2-A, S-2 cloud-free scenes were processed. Scenes from S-1 and S-2 acquired on (almost) the same day were considered as a pair and described in Table 3. On these dates the plants had reached 70% of their maximum height development in the field and had a height corresponding at least to 70% of the full height in order to exclude low PWC values, because when plants are small and have just started their photosynthetic activity, a low value of PWC can be associated with high PRI, especially on hot and sunny days. In the same way, for S-2 data, when the contribution of the soil to the reflectance signal was significant due to low vegetation

fractional cover, we decided to exclude the points where the plants' height was lower than 70% [47,48] compared to the full height. In more detail, the threshold of 70% was introduced in order not to associate low PWC values with high PRI values. When the vegetation has just emerged from the ground, the PWC values are very low while the crop has high photosynthetic activity. Therefore, on hot and sunny days, the PRI values could be comparable to when the plant was in the maturation phase. Therefore, three classification zones were introduced:

**Table 3.** Temporal associations between S-1 and S-2 passes.

| Date S-1 | Date S-2 | Type of Orbit |
|---|---|---|
| 07/07/2022 | 07/07/2022 | Descending |
| 14/07/2022 | 12/07/2022 | Descending |
| 19/07/2022 | 17/07/2022 | Descending |
| 20/07/2022 | 22/07/2022 | Ascending |
| 27/07/2022 | 27/07/2022 | Ascending |
| 01/08/2022 | 01/08/2022 | Ascending |
| 08/08/2022 | 06/08/2022 | Ascending |
| 13/08/2022 | 16/08/2022 | Ascending |
| 25/08/2022 | 26/08/2022 | Ascending |
| 31/08/2022 | 31/08/2022 | Descending |
| 27/07/2023 | 27/07/2023 | Ascending |
| 15/08/2023 | 16/08/2023 | Ascending |
| 26/08/2023 | 26/08/2023 | Descending |
| 07/09/2023 | 05/09/2023 | Descending |
| 12/09/2023 | 10/09/2023 | Descending |
| 13/09/2023 | 15/09/2023 | Ascending |
| 25/09/2023 | 25/09/2023 | Ascending |
| 01/10/2023 | 30/09/2023 | Descending |

Zone (1): High PRI and low PWC: when the small plant had just emerged (in the PWC–PRI plain, at the top left).

Zone (2): High PRI (and a little higher than zone 1) and high PWC: when the plant was growing with considerable PWC variations compared to zone 1 while the PRI variations were not as appreciable (in the PWC–PRI plain, graph at the top right).

Zone (3): Low PRI and low PWC: at the beginning of the senescence phase, consequently the PWC values begin to decrease and also PRI (in a the PWC–PRI plain, at the bottom left).

Consequently, to increase the correlation the points of zone 1 were excluded, otherwise an almost horizontal straight line would have come out. Further studies and insights can be carried out in zone 1, in order to better understand these mechanisms.

Integrating in situ PRI and combining this information with PWC obtained from S-1 data and a series of well-known indices from S-2, which are sensitive to various plant conditions, a more precise and comprehensive investigation of crop health and water status over the two-year study period was achieved.

### *2.3. In Situ Measurements*

SMC was measured using the SPECTRUM-350 TDR probe [49], and vegetation PRI was assessed through the PlantPen PRI210® [50], during the satellite passes. In situ measurements started 20 min before and continued until 20 min after the satellite acquisitions. In more detail, PRI values were obtained by taking three measurements for leaf on four different leaves from a sample of ten sorghum plants (Figure 4). Consequently, we obtained a total of 120 PRI measurements for each satellite pass.



**Figure 4.** A sorghum plant where PRI was measured.

SMC values were obtained by taking three measurements per sample across ten different areas of the field. Given the relatively small size of the fields, a single value of PRI and SMC was associated with each satellite pass. To reduce the influence of potential outliers on ground and remote-sensing measurements, the values of $\sigma^0$, reflectance in the S-2 bands, and PRI over the fields were represented by the median, while SMC values were obtained using the mean, due to the strong spatial homogeneity of the measurements across different field zones. Consequently, each satellite pass was associated with a value of $\sigma^0$ and reflectance corresponding to the in-situ measurements. Additionally, the soil roughness under bare soil conditions or when vegetation was very small was measured, using a needle profilometer to measure correlation length (Lc) and standard deviation of surface height (s) through an image processing script implemented in MATLAB R2022b. Moreover, PWC was obtained by measuring the fresh weight of a sample consisting of three plants in the field, then drying in an oven at 80 °C for 24 h. The plant density in the fields was about 33 plants per $m^2$ in 2022 and 40 per $m^2$ in 2023. PWC was measured once for each pair of consecutive descending–ascending satellite passes, since the water variation over 36 h is negligible [51] and comparable to the intrinsic uncertainties of the instruments.

Here, we will make some considerations about soil conditions with greater SMC values. These values depend on the different depth investigated by the TDR sensor and by C- band SAR, since the first can sense about 15 cm of soil, while the second can sense only the first few cm. In general, the TDR measurements were representative of the surface soil moisture observed by SAR, since the soil moisture profile of the observed field was almost uniform; however, the intense rain events that occurred in the summer after a long dry period created a strong difference between the surface layer (very flooded or muddy), and the subsurface layer, which remained almost dry. In these conditions, TDR measurements cannot be considered representative of the soil layer observed by SAR. We decided, therefore, to discard these values.

### *2.4. Electromagnetic Models*

In order to analyze and interpret the satellite data, some electromagnetic models were employed, including the WCM and the IEM, in combination with the Oh model for estimating cross-polar $\sigma^0$ [35] and the Dobson model for calculating the dielectric permittivity of soil. The WCM considers the canopy and underlying soil separately, allowing the estimation of PWC by accounting the vegetation attenuation effects. In our study, we measured SMC and the variables to estimate PWC that minimize the difference between $\sigma^0$ measured by S-1 and simulated by the WCM by the formula:

$$\sigma^0_{WCM} = B \cdot PWC \cdot \cos\theta_i \cdot [1 - \exp(-2A \cdot PWC \cdot \sec\theta_i)] + \sigma^0_s \cdot \exp(-2A \cdot PWC \cdot \sec\theta_i) \quad (1)$$

where $\theta_i$ = incidence angle, $\sigma^0_s$ = simulated soil backscatter and $A$, $B$ = free parameters. To estimate the parameters A and B, the couple (A, B) that minimizes the difference between $\sigma^0$ measured by S-1 and the one simulated by the WCM was determined. The parameters A and B were estimated within a discrete set of values A = $\{A_1, A_2, A_3, \ldots A_M\}$ and B = $\{B_1, B_2, B_3, \ldots B_N\}$. For each combination of elements from these sets, the absolute difference between $\sigma^0$ measured by S-1 and $\sigma^0{}_{WCM}$ was calculated in linear scale. This process resulted in a matrix of linear differences of $\sigma^0$ with a number of rows corresponding to the cardinality of A (M) and a number of columns corresponding to the cardinality of B (N). The cell with the smallest value indicates the couple (A, B) that minimizes the difference between measured and simulated $\sigma^0$. The A and B extracted for this study were 0.001 $m^2/kg$ and 0.244 $m^2/kg$, respectively, in VH polarization and exponential autocorrelation function for soil roughness estimation. A and B represent attenuations of the electromagnetic wave in vegetation and must be positive. Our results satisfy this condition [13,15]. In VV polarization the estimated PWC values were less reliable due to the higher sensitivity of VV polarization to SMC than VH, as has already been demonstrated in the literature [52] and verified experimentally during the 2022 campaign [37].

## 3. Results

During the two summer seasons the impact of SMC on photosynthetic activity was investigated. As can be noted in Figure 5, where the rainfall data downloaded at [53] were reported, a very dry season occurred during summer 2022 and rainfall arrived shortly before the harvest in the last days of August. In March 2022, the rains were concentrated in only two thunderstorms, whereas, in 2023, rainfall was concentrated in spring and there was a dry September, when the crop was in the senescence phase. The observation revealed that PRI had lower peaks in the summer season of 2022, also indicating reduced photosynthetic activity in response to lower SMC. This behavior is illustrated in Figure 6, where the boxplots of measured PRI and SMC are compared for 2022 and 2023. The boxplots are shown for PRI (left) and SMC (right) for each field and for the entire year. PRI values tend to be higher in 2023 than in 2022 (although with higher dispersion), whereas SMC increases significantly from 2022 to 2023 (although generally reaching low values: 5–10% in 2022 and 10–15% in 2023.

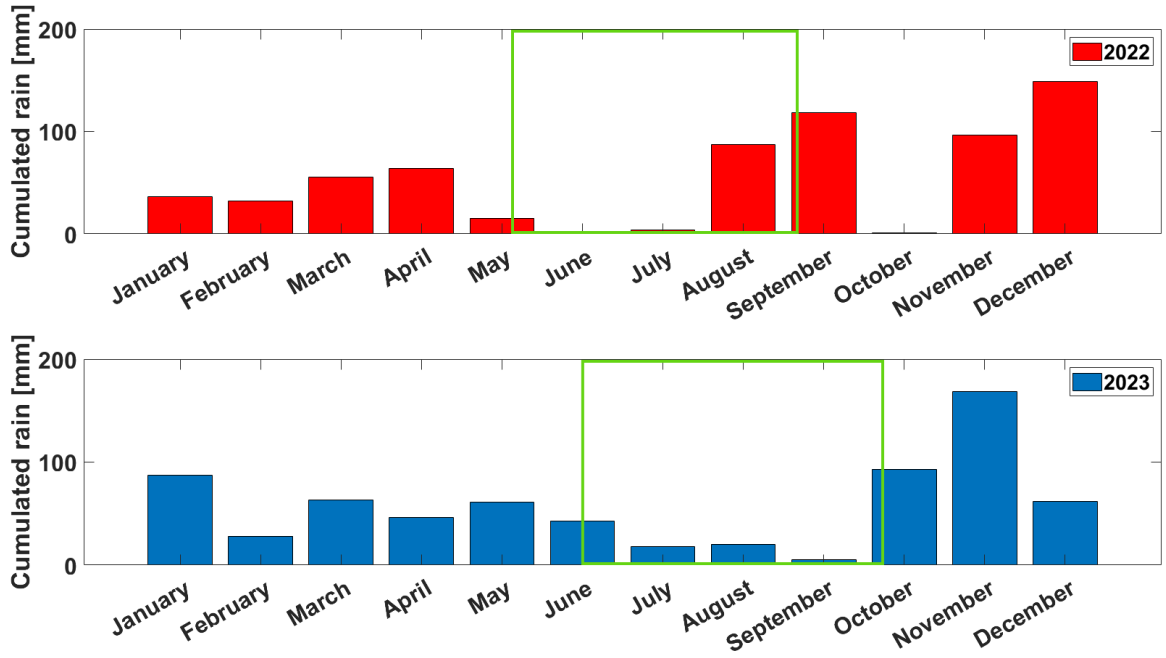



**Figure 5.** Cumulated rainfall during 2022 and 2023. The green boxes indicate the growth cycle of sorghum for each year.

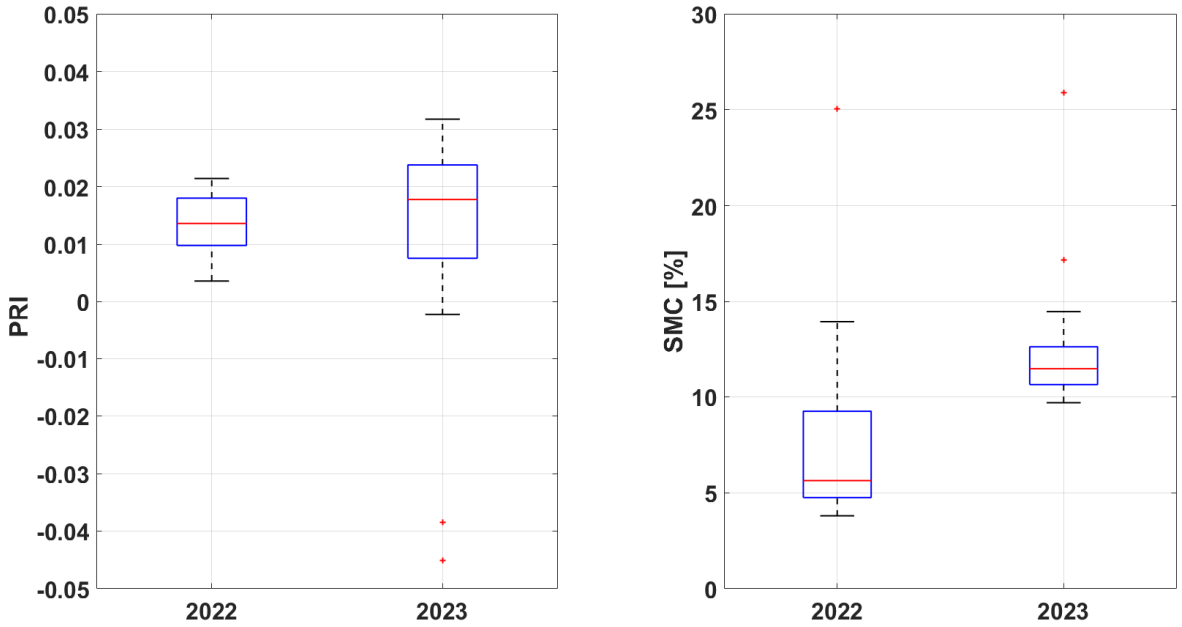



**Figure 6.** Boxplots of PRI (**left**) and SMC (**right**) during 2022 and 2023. PRI intensities are usually lower when the soil is in a dry condition.

To better investigate the water and health status of vegetation, the indices listed in Table 2 were associated with the PRI measurements which were collected simultaneously with the S-2 passes. Figures 7 and 8 show the relationships of the optical indices obtained from S-2 with PRI values measured on the ground in the two years of observation, in the top leaves of vegetation, and all leaves measured, respectively. Given the almost negligible penetration of the optical wavelengths inside the vegetation, the results using only the top leaves of vegetation tend to be better than those obtained using all the leaves.

**Table 4.** Fittings and $R^2$ of the pictures present in Figure 7.

| Index | Regressions | $R^2$ |
|---|---|---|
| NDRE | 7.4594·PRI + 0.2634 | 0.58 |
| RGR | −11.571·PRI + 1.1308 | 0.70 |
| PSRI | −3.3099·PRI + 0.0434 | 0.73 |
| SIPI | −8.4102·PRI + 1.3135 | 0.64 |

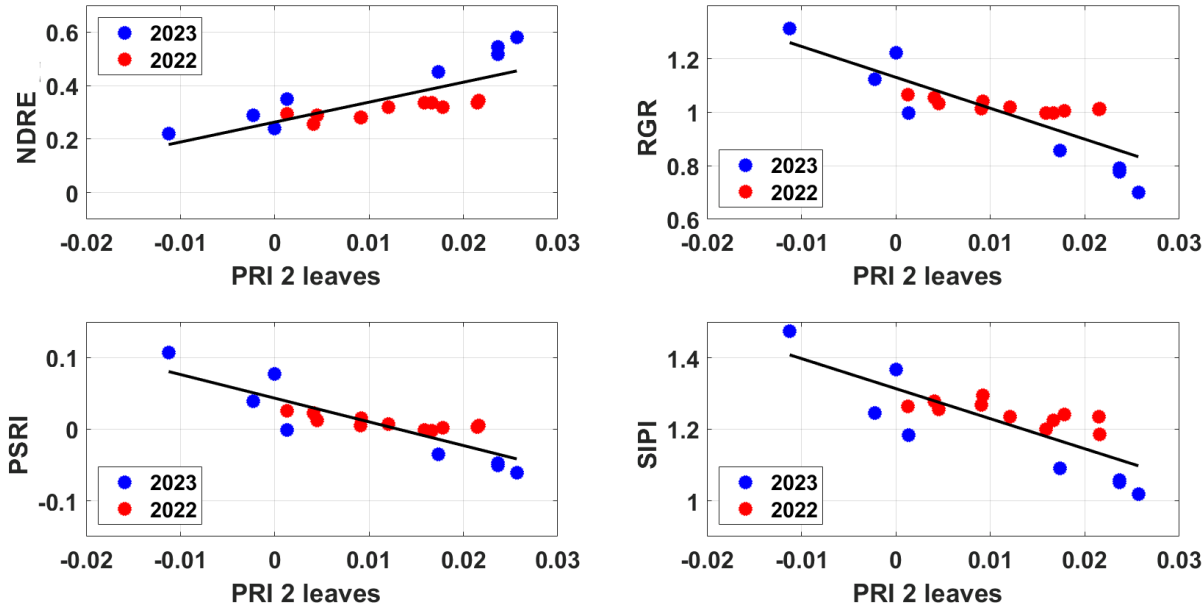



**Figure 7.** Index values obtained from the S-2 bands compared to the foliar PRI measured in the first two leaves of the plant. Data relating to the 2022 seasons, in red, and 2023, in blue. Values of correlations are shown in Table 4.

**Table 5.** Fittings and $R^2$ of the pictures present in Figure 8.

| Index | Fitting | $R^2$ |
|---|---|---|
| NDRE | 3.9302·PRI + 0.3136 | 0.43 |
| RGR | −6.9413·PRI + 1.06 | 0.67 |
| PSRI | −2.0475·PRI + 0.0236 | 0.75 |
| SIPI | −5.0091·PRI + 1.2618 | 0.61 |

Then, the relationship between the PWC derived from S-1 data and the PRI measured in situ was explored to better understand the vegetation water status and its impact on photosynthetic efficiency. The results of Figure 9 show a clear relationship between PWC and PRI, provided that only data collected in well-developed conditions (more than or equal to 70% of the maximum plant height) or the senescence stage are taken into consideration, as already stated in Section 2.2.

To go deeper into this investigation, the relationships between PWC estimated from the S-1 and S-2 indices, already indicated in Table 2, were analyzed. Figure 10 illustrates such relationships, highlighting the effectiveness of integrating SAR and optical remote sensing data for more complete agricultural monitoring.

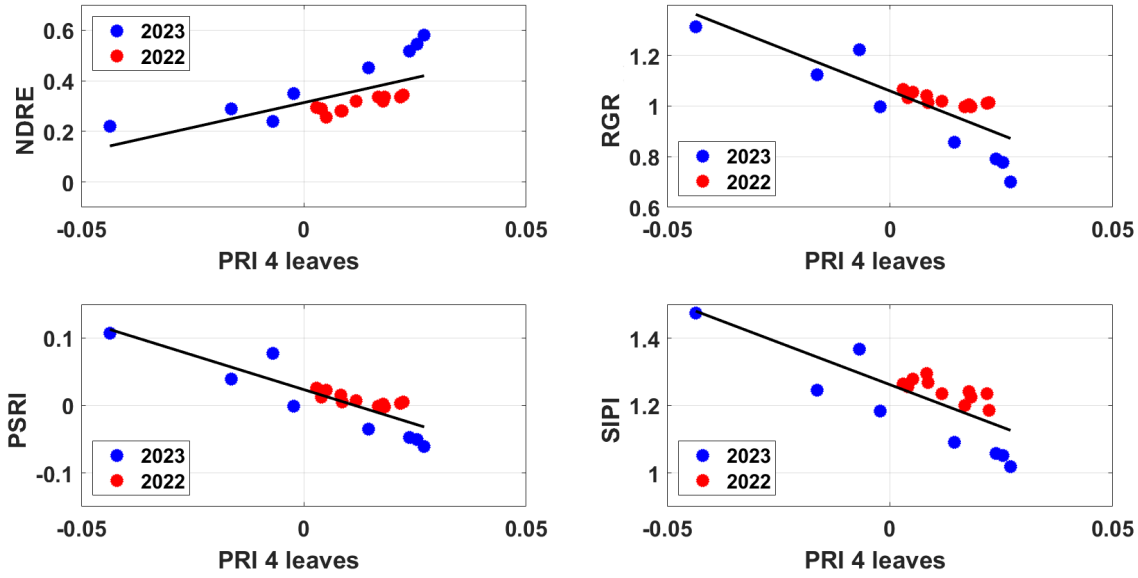



**Figure 8.** Index values obtained from the S-2 bands compared to the leaf PRI measured in the field for all four leaves measured. Data relating to the 2022 seasons, in red, and 2023, in blue. Value of fittings in Table 5.

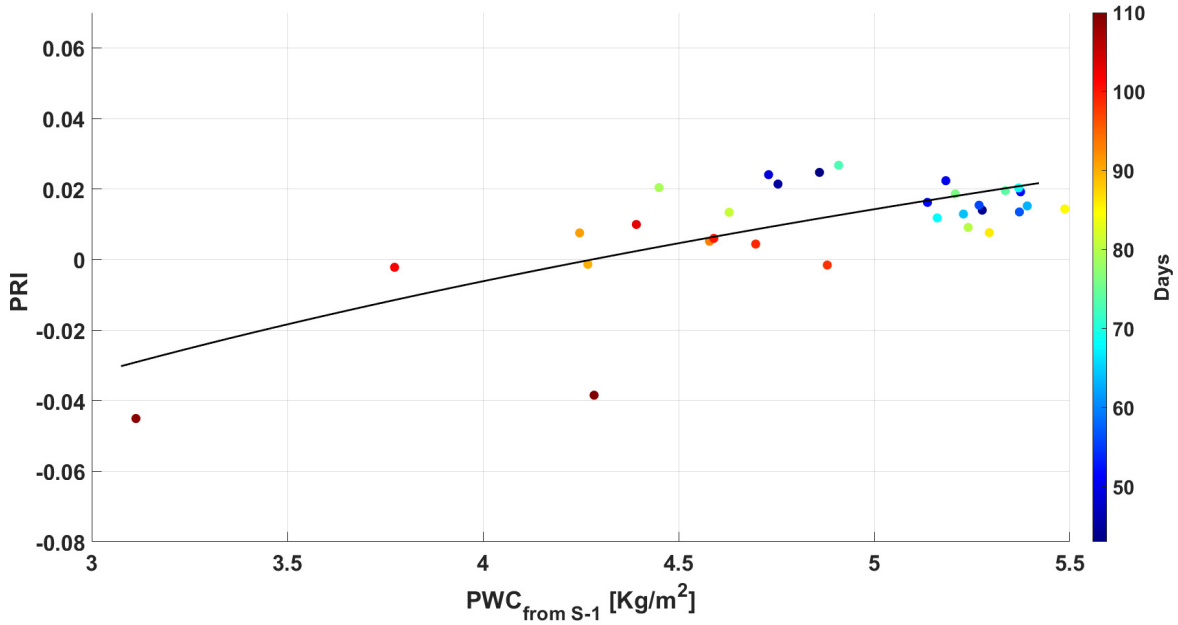



**Figure 9.** PRI measured in the top four leaves as a function of the PWC estimated from $\sigma^0$. The points with similar dry soil conditions (SMC < 15%) were considered, by improving the result in terms of a reduction in the uncertainty of PWC. ($R^2$ = 0.51; PRI = 0.0915·ln(PWC) − 0.133). In the color bars, the days after the sowing of the crop.

**Table 6.** Regressions and $R^2$ of the diagrams of Figure 10.

| Index | Fitting | $R^2$ |
|---|---|---|
| NDRE | 0.0849·PWC − 0.0634 | 0.24 |
| RGR | −0.1664·PWC + 1.8097 | 0.46 |
| PSRI | −0.0505·PWC + 0.2521 | 0.54 |
| SIPI | −0.1191·PWC + 1.7976 | 0.41 |

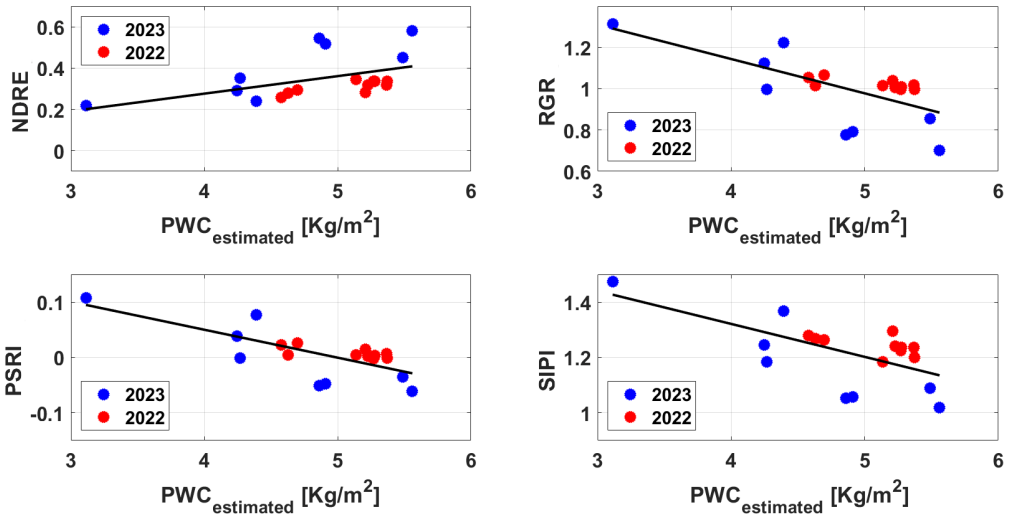



**Figure 10.** Indices obtained from the S-2 bands compared to PWC obtained from the S-1 data through the WCM model. In red the data of 2022 and in blue those of 2023. Regression equations are reported in Table 6.

Among the possible sources of error that affect the correlation between the investigated parameters, we can list the accuracy of the PRI and SMC measuring instruments, the accuracy of SAR measurements, and modeling assumptions in the WCM implementation.

Finally, an analysis was performed to investigate the variations of PWC and PRI [54]. This was achieved by using the difference between ascending and descending orbits of S-1, taking advantage of the different time of their acquisitions (i.e., ascending in the afternoon and descending in the morning). The differences in PWC (ΔPWC) and PRI (ΔPRI) have been computed considering all orbit acquisitions, removing values corresponding to measures carried out in the presence of surface water or mud and thus with extremely high SMC values (Figure 11). We made sure that ΔPWC were not due to variation in plant biomass, by taking into consideration only well-developed plants (in a range of PWC between 1.85 and 6 Kg/m$^2$). From the diagram we can note that there is a rather clear trend between ΔPRI and ΔPWC, thus confirming the ability of both optical and SAR systems in assessing the water status of crops.

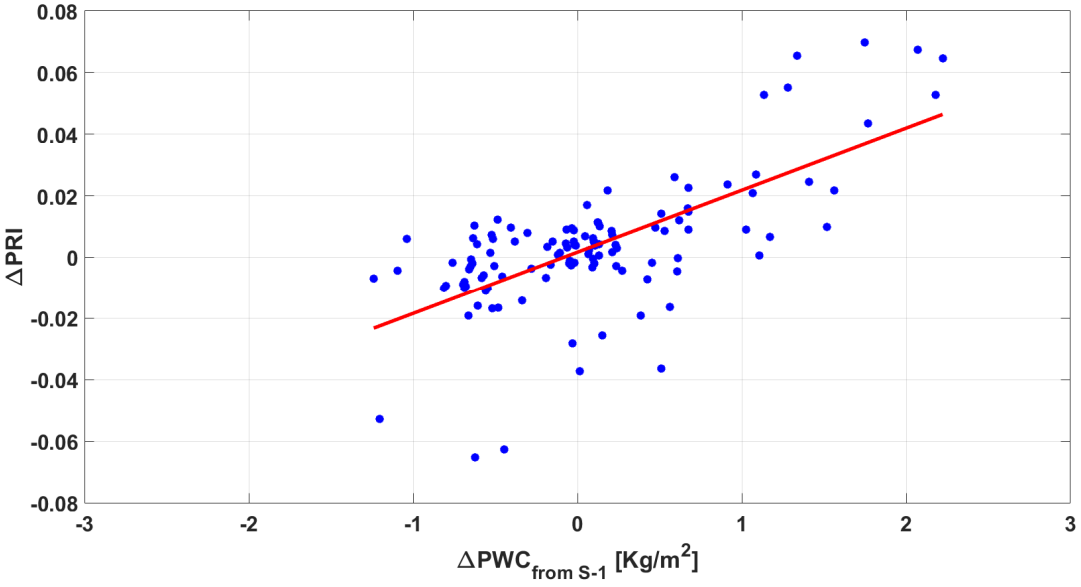



**Figure 11.** Variations between PRI and PWC obtained from morning and afternoon satellite passes and considering dry soil conditions only ($R^2$ = 0.46; ΔPRI = 0.0201·ΔPWC + 0.0017).

## 4. Discussion

The use of both SAR (of S-1) and multispectral (S-2) can provide a robust approach for monitoring crop conditions, particularly for assessing vegetation water status under varying environmental conditions. The study demonstrated that the combination of these data is able to catch the complex interactions between soil and vegetation, providing valuable insights that single-sensor approaches might overlook or fail to evaluate. The relationship between PRI, an index sensitive to changes in the photosynthetic efficiency of plants (measured using a portable device), and SMC (measured on the ground with TDR probes) highlighted how plants react with respect to environmental stress conditions. This finding underscores the potentiality of combining SAR and optical indices to better understand plant–water–health relationships, which is crucial for improving irrigation practices and crop management. Data from S-1 can thus be used to estimate either PWC or SMC, whereas the optical data from S-2 provided complementary information on leaf pigments and leaf water status, enhancing overall accuracy. Given the strong relationship between PRI and S-2 indices, similar information can also be derived using both satellite datasets, avoiding the need for in situ PRI leaf measurements. This novel approach offers a reliable method for identifying the plant water status. By leveraging the complementary strengths of SAR and optical sensors, it is possible to develop more accurate models for predicting crop yield, optimizing water usage, and responding to environmental stressors in almost real time. Furthermore, the analysis of S-1 data across different orbital passes (ascending and descending) highlighted notable temporal variations in PWC, revealing variations in plant status. These variations [55] highlight the sensitivity of SAR measurements to changes in PWC, emphasizing the importance of integrating multi-sensor data. The corresponding observed variations of PRI offer a powerful tool for assessing crop health, particularly in semi-arid regions [56] where water availability is a critical factor. Although PRI cannot be measured from S-2, the correlations found between PRI and some selected optical indices derived from S-2 data confirm the possibility of investigating the water status and stress of crops from satellite. Furthermore, since most agricultural fields are rainfed, these methodologies can be used to understand the local health status of agricultural lands that in recent years have seen increasing damage caused by climate change, such as yield loss [57–59].

In addition to the convergent results already reported, our study also reveals differences that merit further discussion. For instance, our analysis shows that variations in orbital passes (ascending versus descending) can lead to significant differences in the backscatter values due to the anisotropy of agronomic targets and consequently in the derived parameters. Furthermore, although similar correlations between PRI and optical indices have been documented in the literature [60], our integration of in situ PRI measurements with satellite observations occasionally revealed discrepancies. These contradictions could be related to local environmental conditions or variations in crop management practices. Addressing these divergent results is crucial, as it emphasizes the need for a more nuanced understanding of how temporal and spatial factors influence the integration of SAR and optical data for crop monitoring.

## 5. Conclusions

This study highlights the potential of integrating S-1 and S-2 data to investigate the relationship between photosynthetic activity, measured through PRI, and vegetation water content, detected by radar sensors. The results provide new insights into how these parameters are related, even though several aspects remain to be further explored. Specifically, while our analysis confirms the feasibility of using SAR and multispectral data [61] for PRI–PWC monitoring, further studies are needed to consolidate the methodology and assess its applicability across different crop types and environmental conditions. Future

research should focus on refining the temporal and spatial resolution of these integrations, validating the findings with well-established vegetation indices, and exploring how this approach can be effectively implemented in precision agriculture. In particular, a better understanding of the relationships between SAR and optical data and PRI–PWC could lead to improved agricultural management strategies, particularly in the context of water stress monitoring and climate change adaptation. Investigating these dynamics more deeply will be crucial to optimizing irrigation practices and ensuring sustainable agricultural production. The satellite data were compared with in situ measurements of SMC, surface roughness, and plant parameters, as well as leaf PRI measurements. The use of open-source data and products, such as those provided by the European Space Agency's Copernicus platform elaborated in GEE, ensure the full reproducibility of the methodologies developed in this study. The integration of electromagnetic models such as the WCM and IEM allowed for a detailed analysis and interpretation of the obtained information. The comparison of data from very close S-1 and S-2 passes allowed for the assessment of some relationships between optical indices and the daily variations of PWC, which was directly measured in the field. PRI values were associated with several S-2 indices, showing a correlation between these variables, consistent with studies reported in the literature. These comparisons have clearly highlighted the relationships between the analyzed multispectral indices and the vegetation water content, and consequently, the health status of the plants. The analysis also revealed a correlation between the variations in PWC and the xanthophyll cycle, which characterizes the photosynthetic state of the plants. Given PRI's sensitivity to plant health and stress, the study demonstrated that consistent variations in PRI may correspond to changes in water content as measured by satellite sensors. The methodology adopted in this study suggests several paths to follow for future research. One possible direction is the validation of the methodology on a larger scale, for instance by using PRI values obtained from the MODIS satellite platform, although with worse spatial resolutions, in the order of 500 m or 1 km. In any case, the high correlations found between optical indices from S-2 and PRI allow for the possibility of investigating the crop water status directly from satellite. An additional area of investigation could be that represented by the analysis of the problem from a radiometry perspective, as well as the possibility of improving vegetation parameterization using more complex electromagnetic models and potentially for different frequencies. Consequently, additional experimental data and analyses will be necessary to move this research forward.

**Author Contributions:** Conceptualization: S.P. (Simone Pilia), E.P. and G.F.; methodology: S.P. (Simone Pilia); software: S.P. (Simone Pilia) and E.P.; validation: S.P. (Simone Pilia) and G.R.; data curation: S.P. (Simone Pilia), L.S., F.B. and A.L.; formal analysis: F.B.; investigation: E.P., G.R. and A.L.; resources: L.S.; writing—original draft: S.P. (Simone Pilia); writing—review and editing, G.F.; E.S., S.P. (Simone Pettinato) and S.P. (Simonetta Paloscia); supervision: G.F., E.S. and S.P. (Simonetta Paloscia). All authors have read and agreed to the published version of the manuscript.

**Funding:** This research was partially funded by Ente Cassa di Risparmio through the projects "Formazione di nuovi ricercatori esperti nelle tecnologie sviluppate presso IFAC-CNR per agrosensing, diagnostica medica precoce, monitoraggio dell'aria, processi di degrado del patrimonio culturale e del costruito (IFACxFI)", number DIT.AD016.099 and FOE 2020 "Transizione industriale e resilienza delle Società post-Covid19—AGROSENSING", number DIT.AD022.180.

**Data Availability Statement:** The original contributions presented in this study are included in the article. Further inquiries can be directed to the corresponding author.

**Conflicts of Interest:** The authors declare no conflicts of interest. The funders had no role in the design of the study; in the collection, analyses, or interpretation of data; in the writing of the manuscript; or in the decision to publish the results.

## References

1. Furtak, K.; Wolińska, A. The impact of extreme weather events as a consequence of climate change on the soil moisture and on the quality of the soil environment and agriculture—A review. *Catena* **2023**, *231*, 107378. [CrossRef]
2. Donati II, M.; Viaggi, D.; Srdjevic, Z.; Srdjevic, B.; Di Fonzo, A.; Del Giudice, T.; Cimino, O.; Martelli, A.; Dalla Marta, A.; Henke, R.; et al. An analysis of preference weights and setting priorities by irrigation advisory services users based on the analytic hierarchy process. *Agriculture* **2023**, *13*, 1545. [CrossRef]
3. Della Rocca, F.; De Feis, I.; Masiello, G.; Pasquariello, P.; Serio, C. Comparison of the IASI water deficit index and other vegetation indices: The case study of the intense 2022 drought over the Po Valley. In *Remote Sensing of Clouds and the Atmosphere XXVIII*; SPIE: Bellingham, WA, USA, 2023; Volume 12730, pp. 94–107.
4. Farooq, A.; Farooq, N.; Akbar, H.; Hassan, Z.U.; Gheewala, S.H. A critical review of climate change impact at a global scale on cereal crop production. *Agronomy* **2023**, *13*, 162. [CrossRef]
5. Ramat, G.; Santi, E.; Paloscia, S.; Fontanelli, G.; Pettinato, S.; Santurri, L.; Souissi, N.; Da Ponte, E.; Abdel Wahab, M.M.; Khalil, A.A.; et al. Remote sensing techniques for water management and climate change monitoring in drought areas: Case studies in Egypt and Tunisia. *Eur. J. Remote Sens.* **2023**, *56*, 2157335.
6. FAO. *FAO Publications Catalogue 2023*; FAO: Rome, Italy, 2023. [CrossRef]
7. Tian, J.; Zhang, Z.; Philpot, W.D.; Tian, Q.; Zhan, W.; Xi, Y.; Wang, Y.; Zhu, C. Simultaneous estimation of fractional cover of photosynthetic and non-photosynthetic vegetation using visible-near infrared satellite imagery. *Remote Sens. Environ.* **2023**, *290*, 113549. [CrossRef]
8. Thenkabail, P.S.; Smith, R.B.; De Pauw, E. Hyperspectral vegetation indices and their relationships with agricultural crop characteristics. *Remote Sens. Environ.* **2000**, *71*, 158–182.
9. Harries, J.; Carli, B.; Rizzi, R.; Serio, C.; Mlynczak, M.; Palchetti, L.; Maestri, T.; Brindley, H.; Masiello, G. The far-infrared Earth. *Rev. Geophys.* **2008**, *46*. [CrossRef]
10. Wolanin, A.; Camps-Valls, G.; Gómez-Chova, L.; Mateo-García, G.; van der Tol, C.; Zhang, Y.; Guanter, L. Estimating crop primary productivity with Sentinel-2 and Landsat 8 using machine learning methods trained with radiative transfer simulations. *Remote Sens. Environ.* **2019**, *225*, 441–457.
11. Murino, L.; Amato, U.; Carfora, M.F.; Antoniadis, A.; Huang, B.; Menzel, W.P.; Serio, C. Cloud detection of MODIS multispectral images. *J. Atmos. Ocean. Technol.* **2014**, *31*, 347–365.
12. Paloscia, S.; Santi, E.; Fontanelli, G.; Montomoli, F.; Brogioni, M.; Macelloni, G.; Pampaloni, P.; Pettinato, S. The sensitivity of COSMO-SkyMed backscatter to agricultural crop type and vegetation parameters. *IEEE J. Sel. Top. Appl. Earth Obs. Remote Sens.* **2014**, *7*, 2856–2868.
13. Santi, E.; Paloscia, S.; Pettinato, S.; Fontanelli, G.; Mura, M.; Zolli, C.; Maselli, F.; Chiesi, M.; Bottai, L.; Chirici, G. The potential of multifrequency SAR images for estimating forest biomass in Mediterranean areas. *Remote Sens. Environ.* **2017**, *200*, 63–73. [CrossRef]
14. Macelloni, G.; Paloscia, S.; Pampaloni, P.; Marliani, F.; Gai, M. The relationship between the backscattering coefficient and the biomass of narrow and broad leaf crops. *IEEE Trans. Geosci. Remote Sens.* **2001**, *39*, 873–884. [CrossRef]
15. Paloscia, S.; Pettinato, S.; Santi, E.; Notarnicola, C.; Pasolli, L.; Reppucci, A. Soil moisture mapping using Sentinel-1 images: Algorithm and preliminary validation. *Remote Sens. Environ.* **2013**, *134*, 234–248.
16. Khati, U.; Lavalle, M.; Singh, G. The role of time-series L-band SAR and GEDI in mapping sub-tropical above-ground biomass. *Front. Earth Sci.* **2021**, *9*, 752254.
17. Hensley, S.; Van Zyl, J.; Lavalle, M.; Neumann, M.; Michel, T.; Muellerschoen, R.; Pinto, N.; Simard, M.; Moghaddam, M. L-band and P-band studies of vegetation at JPL. In Proceedings of the 2015 IEEE Radar Conference, Johannesburg, South Africa, 27–30 October 2015; pp. 516–520.
18. Potin, P.; Rosich, B.; Grimont, P.; Miranda, N.; Shurmer, I.; O'Connell, A.; Torres, R.; Krassenburg, M. Sentinel-1 mission status. In Proceedings of the EUSAR 2016: 11th European Conference on Synthetic Aperture Radar, Hamburg, Germany, 6–9 June 2016; pp. 1–6.
19. Segarra, J.; Buchaillot, M.L.; Araus, J.L.; Kefauver, S.C. Remote sensing for precision agriculture: Sentinel-2 improved features and applications. *Agronomy* **2020**, *10*, 641. [CrossRef]
20. Xue, J.; Su, B. Significant remote sensing vegetation indices: A review of developments and applications. *J. Sens.* **2017**, *2017*, 1353691. [CrossRef]
21. Gamon, J.A.; Penuelas, J.; Field, C.B. A narrow-waveband spectral index that tracks diurnal changes in photosynthetic efficiency. *Remote Sens. Environ.* **1992**, *41*, 35–44.

22. Peñuelas, J.; Filella, I.; Gamon, J.A. Assessment of photosynthetic radiation-use efficiency with spectral reflectance. *New Phytol.* **1995**, *131*, 291–296.
23. Garbulsky, M.F.; Peñuelas, J.; Gamon, J.; Inoue, Y.; Filella, I. The photochemical reflectance index (PRI) and the remote sensing of leaf, canopy and ecosystem radiation use efficiencies: A review and meta-analysis. *Remote Sens. Environ.* **2011**, *115*, 281–297. [CrossRef]
24. Zhang, C.; Filella, I.; Garbulsky, M.F.; Peñuelas, J. Affecting factors and recent improvements of the photochemical reflectance index (PRI) for remotely sensing foliar, canopy and ecosystemic radiation-use efficiencies. *Remote Sens.* **2016**, *8*, 677. [CrossRef]
25. Gamon, J.A.; Kovalchuck, O.; Wong CY, S.; Harris, A.; Garrity, S.R. Monitoring seasonal and diurnal changes in photosynthetic pigments with automated PRI and NDVI sensors. *Biogeosciences* **2015**, *12*, 4149–4159. [CrossRef]
26. Garbulsky, M.F. Remote estimation of carbon dioxide uptake of terrestrial ecosystems. *Nat. Preced.* **2007**. [CrossRef]
27. Zarco-Tejada, P.J.; Hornero, A.; Hernández-Clemente, R.; Beck, P.S.A. Understanding the temporal dimension of the red-edge spectral region for forest decline detection using high-resolution hyperspectral and Sentinel-2a imagery. *ISPRS J. Photogramm. Remote Sens.* **2018**, *137*, 134–148. [CrossRef]
28. Mateo-Sanchis, A.; Piles, M.; Muñoz-Marí, J.; Adsuara, J.E.; Pérez-Suay, A.; Camps-Valls, G. Synergistic integration of optical and microwave satellite data for crop yield estimation. *Remote Sens. Environ.* **2019**, *234*, 111460. [CrossRef]
29. Attema EP, W.; Ulaby, F.T. Vegetation modeled as a water cloud. *Radio Sci.* **1978**, *13*, 357–364. [CrossRef]
30. Baghdadi, N.; El Hajj, M.; Zribi, M.; Bousbih, S. Calibration of the water cloud model at C-band for winter crop fields and grasslands. *Remote Sens.* **2017**, *9*, 969. [CrossRef]
31. Gao, Q.; Zribi, M.; Escorihuela, M.J.; Baghdadi, N. Synergetic use of Sentinel-1 and Sentinel-2 data for soil moisture mapping at 100 m resolution. *Sensors* **2017**, *17*, 1966. [CrossRef] [PubMed]
32. Bao, X.; Zhang, R.; He, X.; Shama, A.; Yin, G.; Chen, J.; Zhang, H.; Liu, G. An Integrated Time-Series Relative Soil Moisture Monitoring Method Based on a SAR Backscattering Model. *IEEE J. Sel. Top. Appl. Earth Obs. Remote Sens.* **2024**, *18*, 2137–2156. [CrossRef]
33. Santi, E.; Paloscia, S.; Pettinato, S.; Entekhabi, D.; Alemohammad, S.H.; Konings, A.G. Integration of passive and active microwave data from SMAP, AMSR2 and Sentinel-1 for Soil Moisture monitoring. In Proceedings of the 2016 IEEE International Geoscience and Remote Sensing Symposium (IGARSS), Beijing, China, 10–15 July 2016; pp. 5252–5255.
34. Fung, A.K. *Microwave Scattering and Emission Models and Their Applications*; Artech House Publishers: London, UK, 1994.
35. Oh, Y.; Sarabandi, K.; Ulaby, F.T. An empirical model and an inversion technique for radar scattering from bare soil surfaces. *IEEE Trans. Geosci. Remote Sens.* **1992**, *30*, 370–381. [CrossRef]
36. Dobson, M.C.; Ulaby, F.T.; Hallikainen, M.T.; El-Rayes, M.A. Microwave dielectric behavior of wet soil-Part II: Dielectric mixing models. *IEEE Trans. Geosci. Remote Sens.* **1985**, *23*, 35–46. [CrossRef]
37. Pilia, S.; Fontanelli, G.; Santurri, L.; Ramat, G.; Baroni, F.; Santi, E.; Lapini, A.; Pettinato, S.; Paloscia, S. Data integration of Sentinel-1 and Sentinel-2 for evaluating vegetation biomass and water status. In Proceedings of the 2023 IEEE International Workshop on Metrology for Agriculture and Forestry (MetroAgriFor), Pisa, Italy, 6–8 November 2023; pp. 694–698.
38. Pilia, S.; Baroni, F.; Fontanelli, G.; Ramat, G.; Palchetti, E.; Paloscia, S.; Pettinato, S.; Santi, E.; Santurri, L. Soil and Vegetation Water Status Monitoring by Integrating Optical and Microwave Satellite Data. In Proceedings of the IGARSS 2024-2024 IEEE International Geoscience and Remote Sensing Symposium, Athens, Greece, 7–12 July 2024; pp. 1470–1473.
39. Available online: https://world-soils.com/ (accessed on 30 August 2024).
40. Available online: https://www.esa.int/Applications/Observing_the_Earth/Copernicus/Sentinel-1/Mission_ends_for_Copernicus_Sentinel-1B_satellite (accessed on 26 April 2025).
41. Barnes, E.M.; Clarke, T.R.; Richards, S.E.; Colaizzi, P.D.; Haberland, J.; Kostrzewski, M.; Waller, P.; Choi, C.; Riley, E.; Thompson, T.; et al. Coincident detection of crop water stress, nitrogen status and canopy density using ground based multispectral data. In Proceedings of the Fifth International Conference on Precision Agriculture, Bloomington, MN, USA, 16–19 July 2000; Volume 1619, No. 6.
42. Gamon, J.A.; Surfus, J.S. Assessing leaf pigment content and activity with a reflectometer. *New Phytol.* **1999**, *143*, 105–117. [CrossRef]
43. Merzlyak, M.N.; Gitelson, A.A.; Chivkunova, O.B.; Rakitin, V.Y. Non-destructive optical detection of pigment changes during leaf senescence and fruit ripening. *Physiol. Plant.* **1999**, *106*, 135–141. [CrossRef]
44. Penuelas, J.; Baret, F.; Filella, I. Semi-empirical indices to assess carotenoids/chlorophyll a ratio from leaf spectral reflectance. *Photosynthetica* **1995**, *31*, 221–230.
45. Gorelick, N.; Hancher, M.; Dixon, M.; Ilyushchenko, S.; Thau, D.; Moore, R. Google Earth Engine: Planetary-scale geospatial analysis for everyone. *Remote Sens. Environ.* **2017**, *202*, 18–27. [CrossRef]
46. Clemente, J.P.; Fontanelli, G.; Ovando, G.G.; Roa, Y.L.B.; Lapini, A.; Santi, E. Google Earth Engine: Application of algorithms for remote sensing of crops in Tuscany (Italy). In Proceedings of the 2020 IEEE Latin American GRSS & ISPRS Remote Sensing Conference (LAGIRS), Santiago, Chile, 22–26 March 2020; pp. 195–200.

47. Cai, Y.; Zhang, M.; Lin, H. Estimating the urban fractional vegetation cover using an object-based mixture analysis method and Sentinel-2 MSI imagery. *IEEE J. Sel. Top. Appl. Earth Obs. Remote Sens.* **2020**, *13*, 341–350. [CrossRef]
48. Andreatta, D.; Gianelle, D.; Scotton, M.; Dalponte, M. Estimating grassland vegetation cover with remote sensing: A comparison between Landsat-8, Sentinel-2 and PlanetScope imagery. *Ecol. Indic.* **2022**, *141*, 109102. [CrossRef]
49. Available online: https://www.specmeters.com/FieldScout-TDR350-Soil-Moisture-Meter (accessed on 30 August 2024).
50. Available online: https://handheld.psi.cz/products/plantpen-ndvi-and-pri/ (accessed on 30 August 2024).
51. Konings, A.G.; Rao, K.; Steele-Dunne, S.C. Macro to micro: Microwave remote sensing of plant water content for physiology and ecology. *New Phytol.* **2019**, *223*, 1166–1172. [CrossRef]
52. Ulaby, F.T.; Moore, R.K.; Fung, A.K. *Microwave Remote Sensing: Active and Passive. Volume 2-Radar Remote Sensing and Surface Scattering and Emission Theory*; NTRS: Hilversum, The Netherlands, 1982.
53. Available online: https://www.lamma.toscana.it/meteo/osservazioni-e-dati/dati-stazioni (accessed on 26 April 2025).
54. Takala, T.L.; Mõttus, M. Spatial variation of canopy PRI with shadow fraction caused by leaf-level irradiation conditions. *Remote Sens. Environ.* **2016**, *182*, 99–112. [CrossRef]
55. Ouaadi, N.; Jarlan, L.; Ezzahar, J.; Khabba, S.; Le Dantec, V.; Rafi, Z.; Zribi, M.; Frison, P.L. Water stress detection over irrigated wheat crops in semi-arid areas using the diurnal differences of Sentinel-1 backscatter. In Proceedings of the 2020 Mediterranean and Middle-East Geoscience and Remote Sensing Symposium (M2GARSS), Tunis, Tunisia, 9–11 March 2020; pp. 306–309.
56. Rockström, J.; Karlberg, L.; Wani, S.P.; Barron, J.; Hatibu, N.; Oweis, T.; Bruggeman, A.; Farahani, J.; Qiang, Z. Managing water in rainfed agriculture—The need for a paradigm shift. *Agric. Water Manag.* **2010**, *97*, 543–550. [CrossRef]
57. Available online: https://joint-research-centre.ec.europa.eu/european-and-global-drought-observatories/current-drought-situation-europe_en (accessed on 3 September 2024).
58. Amiri, M.A.; Gocic, M. Analysis of temporal and spatial variations of drought over Serbia by investigating the applicability of precipitation-based drought indices. *Theor. Appl. Climatol.* **2023**, *154*, 261–274. [CrossRef]
59. Edwards, B.; Gray, M.; Hunter, B. The social and economic impacts of drought. *Aust. J. Soc. Issues* **2019**, *54*, 22–31. [CrossRef]
60. Dotzler, S.; Hill, J.; Buddenbaum, H.; Stoffels, J. The potential of EnMAP and Sentinel-2 data for detecting drought stress phenomena in deciduous forest communities. *Remote Sens.* **2015**, *7*, 14227–14258. [CrossRef]
61. Baup, F.; Fieuzal, R.; Ygorra, B.; Frappart, F.; Riazanoff, S.; Martin-Comte, A.; Gorrab, A. 6-Years of Sar (Sentinel-1) and Optical (Sentinel 2, Landsat-8) Acquisitions Over Agricultural Surfaces in Southwestern, France. 2025. Available online: https://papers.ssrn.com/sol3/papers.cfm?abstract_id=5078835 (accessed on 26 April 2025).


**Disclaimer/Publisher's Note:** The statements, opinions and data contained in all publications are solely those of the individual author(s) and contributor(s) and not of MDPI and/or the editor(s). MDPI and/or the editor(s) disclaim responsibility for any injury to people or property resulting from any ideas, methods, instructions or products referred to in the content.